On the Design of Passive Resonant Circuits to Measure Local Pulse Wave Velocity in a Stent

Jonathan Schächtele

***Abstract*—In-stent restenosis is a frequent complication after stent implantation. This article investigates the design of a passive sensor system to be integrated into a stent for the detection of an in-stent restenosis by measuring the local pulse wave velocity (PWV). The proposed system uses two resonant circuits consisting of a capacitive pressure sensor and a coil as transponders. The pressure sensors are located at the proximal and distal end of the stent. An alternating external magnetic field with a constant frequency is applied such that the resonance frequencies of the transponders cross the excitation frequency when the pulse wave passes. The time delay between the resonances at the transponders can be captured to obtain the PWV. A model for the measurement system and a correlation between transponder design parameters and minimal resolvable time delay are derived. This correlation is based on the criterion that the 3dB bandwidth of the transponder resonances may not overlap in the measurement time interval. This correlation can be used to design and analyze a transponder system for the proposed measurement system. In an experiment, in which the pressure sensors have been emulated by varactor diodes, it could be shown that the model is valid and that the criterion is suitable. Finally, the relevant design parameters of the transponders have been identified and their limitations investigated.**

***Index Terms*—passive resonant circuits, resonant sensors, implantable, inductive coupling, pulse transit time, pulse wave velocity, wireless, blood flow, transponder, passive telemetry**

I. Introduction

VASCULAR diseases are a major health concern in industrial countries. A very common manifestation is arteriosclerosis: a hardening and thickening of the blood vessel walls. It can have different causes, e.g. deposition of calcium in the vessel walls or deposition of plaque inside the vessel lumen. Arteriosclerosis can lead to an occlusion of the vessel, a stenosis, that causes a shortage in blood supply (ischemia) and, in worst case, provokes a myocardial infarction [1]. One common procedure to treat arteriosclerosis is implanting a mechanical support, a stent, in order to open and stabilize the vessel from the inside. However, in many patients[1] a restenosis occurs [2], i.e. the vessel lumen is considerably reduced again due to excess cell growth[2]. The mechanisms for this complication are not yet fully understood, but inflammatory responses probably play a key role [2]. The body's response is not always considered harmful: A thin coverage of the stent with endothelial cells is desirable, as it smoothens the inner surface of the vessel and is supposed to reduce the risk of thrombosis [3], [4]. The usual follow-up procedure is to take clinical history every three to six months [5], but not all patients are symptomatic. Currently there is no non-invasive and reliable method to detect in-stent restenosis [6].

Given these issues, an apparent solution is to integrate a sensor system into the stent that enables a reliable and continuous monitoring of the site. Several research groups investigated such solutions, and great progress has been made. Chow *et al.* designed a wirelessly powered pressure sensor to be embedded in a stent [7]. Takahata *et al.* pursued an approach to measure pressure and flow velocity inside the stent with a sensor system that only needs passive components at the implanted side, which makes it potentially cheap and small [8], [9]. They also proposed to use the stent itself as an antenna. Both approaches have the drawback that they rely on absolute pressures or pressure differences. If the sensors are covered with endothelial cells or plaque, the measured values will be corrupted. Green *et al.* pursued a different method to detect sludge in a biliary stent [10]–[13]. They integrated a magnetoelastic mechanical resonator in the stent which was excited via a magnetic field. Any mass loading induced by deposit changes its resonance frequency. Viswanath *et al.* refined this principle further to improve the integration in arterial stents [14]. This principle also only requires passive components. But, just as the pressure measurement, it is prone to be disturbed by cell coverage.

Therefore, the approach investigated in this article is based on the acquisition of the local pulse wave velocity (PWV) inside the stent instead of pressure, which was initially proposed in [15], [16]. It was also inspired by the before mentioned work and the fact that measurement of the mean carotid-femoral pulse wave velocity (PWV) is considered the "gold-standard" for the assessment of arterial stiffness among cardiologists [17].

The pulse wave propagates through the vascular system with every heart beat. The PWV denotes the speed of this wave, and can be described approximately by the Moens Korteweg equation [18, p. 57], [19]:

$$\mathrm{PWV} = \sqrt{\frac{Eh}{2\rho R}} \tag{1}$$

In this equation, E denotes the Young's modulus of the vessel wall, h the wall thickness, ρ the blood density, and R the vessel radius. A restenosis thickens and stiffens the stent conjointly. Both effects lead to an increased PWV. Thus, an increase of local PWV is an indication for restenosis inside the stent.

To measure PWV, a wireless system similar to [9] is proposed: Two capacitive pressure sensors are integrated into

J. Schächtele is with the Fraunhofer Project Group for Automation in Medicine and Biotechnology at the Fraunhofer Institute for Manufacturing Engineering and Automation, Theodor-Kutzer-Ufer 1-3, 68167 Mannheim, Germany, e-mail: jonathan.schaechtele@ipa.fraunhofer.de.

[1]Depending on the type of stent under observation up to 30 % [2]

[2]A clinical restenosis is usually defined as a decrease of the vessel diameter by 50 % or more. [2]

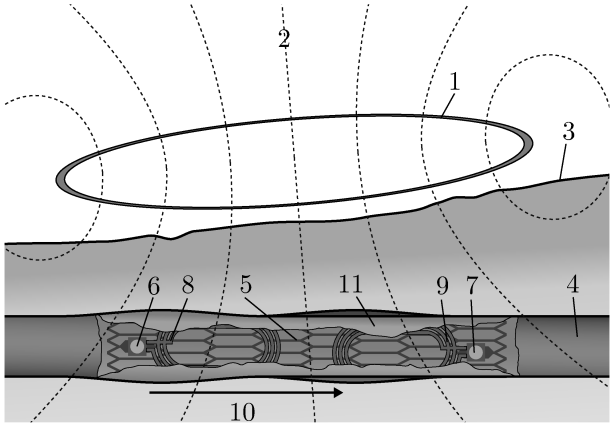

Fig. 1. Concept of the PWV measurement system; 1) external transceiver coil, 2) magnetic field, 3) body surface, 4) blood vessel, 5) stent, 6) sensor 1 (proximal), 7) sensor 2 (distal), 8) coil 1, 9) coil 2, 10) propagation direction of the pulse wave, 11) Plaque

the stent at both the proximal and the distal end. Each of them is coupled with an individual coil forming two LC resonators. These will be referred to as 'the transponders' throughout this article. An external readout unit with a transceiver coil generates a magnetic field and detects the change in impedance when one of the transponders is in resonance. A schematic set-up of the described system is shown in Fig. 1. The innovation of the method is to use the transponders to detect the instant of arrival of the pulse wave instead of measuring absolute pressures or pressure differences. This approach is expected to be more robust against light coverage of the sensors.

The purpose of this article is to model the electromechanical system from the pressure sensors to the inductive transmission, investigate the implications of this approach on the electrical design of the transponders and validate the model and the findings of the investigation by simulations and measurements.

II. Pulse wave detection principle

The transponder resonance frequency f_{res} depends on the pressure at the sensor as follows:

$$f_{\mathrm{res}} = \frac{1}{2\pi\sqrt{LC(p)}}\,. \tag{2}$$

In this equation, L is the inductance of the coil and $C(p)$ is the capacitance of the sensor that depends on the pressure p.

Instead of sweeping a frequency range with the generated field to track the resonance frequency, the concept is to excite with a constant frequency during measurement. The transponder circuits and the constant frequency, denoted observation frequency f_{obs}, are designed and chosen such that during a pulse cycle the resonance frequencies $f_{\mathrm{res},1}$ and $f_{\mathrm{res},2}$ of the transponders cross the observation frequency f_{obs}. The time between the resonances is recorded. Omitting a sweep is expected to reduce measurement time and consequently to increase temporal resolution.

The concept is illustrated in Fig. 1. It does not necessarily show a favorable arrangement, but is suitable to explain the

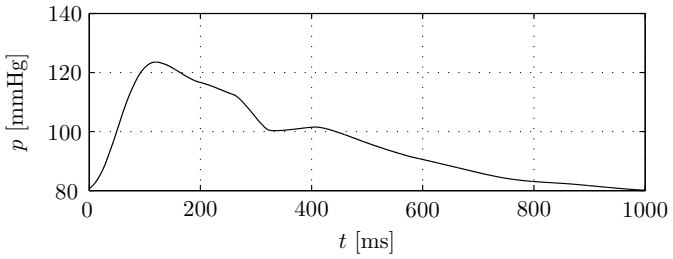

Fig. 2. Typical pulse pressure curve obtained at the common carotid artery [20] (values relative to atmospheric pressure)

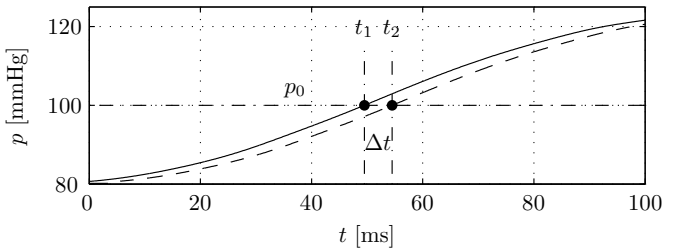

Fig. 3. Detail of the pulse pressure curve; solid line: pressure at proximal sensor, dashed line: pressure at distal sensor

operating principle[3]. It is assumed that there are two identical transponders inside the stent. Their pressure sensors have an axial distance d along the stent. It is also assumed, that a pulse with the typical pressure curve $p(t)$ in Fig. 2 is traveling through the vessel. Due to wave propagation, the pulse curve appears at sensor 2 with a delay of the transit time Δt compared to sensor 1, where

$$\Delta t = \frac{d}{\mathrm{PWV}}\,. \tag{3}$$

Both transponders are in resonance with f_{obs} at the same pressure p_0 described by

$$f_{\mathrm{obs}} = \frac{1}{2\pi\sqrt{LC(p_0)}}\,. \tag{4}$$

The current induced in the transponder at resonance creates a magnetic field that overlays the generated field of the transceiver coil. This causes the impedance at the transceiver coil terminal to change, which can be detected. The effect will be referred to as the 'triggering condition' throughout this article. When p_0 is chosen reasonably (somewhere between minimum and maximum value of the pulse pressure curve), the triggering condition occurs at least twice during the pulse cycle for each transponder: at the rising and at the falling edge. The measurement of the time delay preferably takes place at the rising edge at the beginning of the pressure curve where it usually has a large gradient. Fig. 3 shows a magnification of this region, together with the delayed curve expected at sensor 2 (dashed), a triggering pressure p_0 (in this case $100\,\mathrm{mmHg}$), the triggering times t_1 and t_2 and the delay between the resonances at the two transponders Δt.

[3]E.g. the area, that the transponder coils enclose, should be maximized in order to maximize inductive coupling.

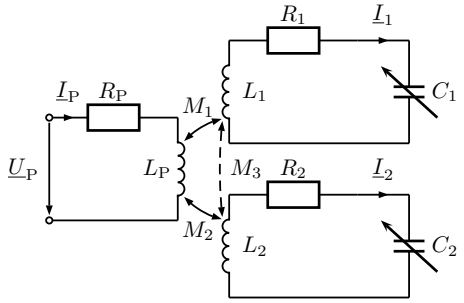

Fig. 4. Equivalent circuit of the measurement system consisting of the transponders and a transceiver coil

III. Model of the measurement system

Fig. 4 shows an equivalent circuit of the proposed wireless measurement system, which resembles the one shown in [8]. For a single transponder similar models have been investigated repeatedly in literature (e.g. [21], [22]), but here it has been extended for two transponders. The inductance L_P together with the resistance R_P model the transceiver coil of the external unit. The implanted transponders are represented by the variable capacitances C_i and the inductances L_i, where the index $i \in \{1, 2\}$ denotes the two sensors. R_i incorporates the resistance of the coils and the equivalent series resistance of the capacitive sensors. Parasitic inductances and capacitances are neglected, given that the operating frequency should be significantly lower than the self-resonances of the components. M_i denotes the mutual inductances between the transceiver and transponder coils. The mutual inductance M_3 between L_1 and L_2 is unwanted and should be kept small by design, but can not be avoided in a real set-up. Applying Kirchhoff's voltage law to the circuit model leads to the system of equations:

$$\begin{pmatrix} \underline{U}_\mathrm{P} \\ 0 \\ 0 \end{pmatrix} = \begin{pmatrix} \underline{A}_{11} & \underline{A}_{12} & \underline{A}_{13} \\ \underline{A}_{21} & \underline{A}_{22} & \underline{A}_{23} \\ \underline{A}_{31} & \underline{A}_{32} & \underline{A}_{33} \end{pmatrix} \cdot \begin{pmatrix} \underline{I}_\mathrm{P} \\ \underline{I}_1 \\ \underline{I}_2 \end{pmatrix} \tag{5}$$

with

$$\begin{aligned} \underline{A}_{11} &= R_\mathrm{P} + \mathrm{j}\omega L_\mathrm{P} \\ \underline{A}_{12} &= -\mathrm{j}\omega M_1 \\ \underline{A}_{13} &= -\mathrm{j}\omega M_2 \\ \underline{A}_{21} &= -\mathrm{j}\omega M_1 \\ \underline{A}_{22} &= R_1 + \frac{1}{\mathrm{j}\omega C_1} + \mathrm{j}\omega L_1 \\ \underline{A}_{23} &= \mathrm{j}\omega M_3 \\ \underline{A}_{31} &= -\mathrm{j}\omega M_2 \\ \underline{A}_{32} &= \mathrm{j}\omega M_3 \\ \underline{A}_{33} &= R_2 + \frac{1}{\mathrm{j}\omega C_2} + \mathrm{j}\omega L_2 \quad \text{and} \\ \omega &= 2\pi f\,. \end{aligned} \tag{6}$$

From these equations, the input impedance at the transceiver coil Z_P can be obtained:

$$\underline{Z}_\mathrm{P} = \frac{\underline{U}_\mathrm{P}}{\underline{I}_\mathrm{P}} = \frac{\det \begin{pmatrix} \underline{A}_{11} & \underline{A}_{12} & \underline{A}_{13} \\ \underline{A}_{21} & \underline{A}_{22} & \underline{A}_{23} \\ \underline{A}_{31} & \underline{A}_{32} & \underline{A}_{33} \end{pmatrix}}{\det \begin{pmatrix} \underline{A}_{22} & \underline{A}_{23} \\ \underline{A}_{32} & \underline{A}_{33} \end{pmatrix}}\,. \tag{7}$$

IV. Requirements on the transponder circuits

In order to distinguish between the two resonances of the transponder circuits it is critical that their peaks do not overlap in the measurement time interval T_M. Therefore, an important measure is the difference between the resonance frequencies of the transponders

$$\begin{aligned} \Delta f_\mathrm{res}(t) &= |f_{\mathrm{res},2}(t) - f_{\mathrm{res},1}(t)| \\ &= \left| \frac{1}{2\pi\sqrt{L_2 C_2(t)}} - \frac{1}{2\pi\sqrt{L_1 C_1(t)}} \right| \end{aligned} \tag{8}$$

which is time-dependent. In $T_\mathrm{M} = [t_1, t_2]$, where t_1 and t_2 are the triggering times at the rising edge of the pulse curve as shown in Fig. 3, this measure may not drop below a value that depends on the bandwidth of the peaks.

A reasonable design criterion is to require that the $3\,\mathrm{dB}$ bands around the resonance frequencies do not overlap[4]. For a weakly dampened resonant circuit the $3\,\mathrm{dB}$ band extends almost symmetrically around the resonance frequency[5]. This leads to the criterion

$$\frac{1}{2} \cdot (B_1 + B_2) \leq \Delta f_{\mathrm{res,min}} \tag{9}$$

where B_1 and B_2 are the $3\,\mathrm{dB}$ bandwidths of the transponders, and $\Delta f_{\mathrm{res,min}}$ is the minimum distance between the resonance frequencies in T_M

$$\Delta f_{\mathrm{res,min}} = \min \left\{ \Delta f_\mathrm{res}(t) \mid t \in T_\mathrm{M} \right\}\,. \tag{10}$$

Capacitive pressure sensors usually have an increasing characteristic, meaning that a higher pressure p at the membrane causes a higher capacitance C. Thus, as the pressure is rising within T_M, the resonance frequencies of the transponders decrease. While they decrease they cross the frequency of the generated field: the proximal sensor 1 at t_1 and the distal sensor 2 at t_2 (see Fig. 3). Therefore the relation

$$f_{\mathrm{res},1}(t) \leq f_\mathrm{obs} \leq f_{\mathrm{res},2}(t) \quad \forall t \in T_\mathrm{M} \tag{11}$$

applies.

To investigate the implications resulting from requirement (9) an expression for $\Delta f_{\mathrm{res,min}}$ is needed. For this, the pulse pressure curve and the characteristic of the capacitive pressure sensors are linearized around the triggering condition $f_{\mathrm{res},i} = f_\mathrm{obs}$. The triggering condition can be given as

$$f_\mathrm{obs} = \frac{1}{2\pi\sqrt{L_i C_{0,i}}} \tag{12}$$

[4]It is common to use this bandwidth definition in electrical engineering [23, p. 23].

[5]If the quality factor Q is greater than 50, the deviation of the ratio $(f_2 - f_0)/(f_0 - f_1)$ from unity is less than $1\,\%$, with f_1 and f_2 being the $3\,\mathrm{dB}$ frequencies left and right of the resonance frequency f_0.

with the capacitance at the triggering condition

$$C_{0,i} = \frac{1}{L_i \cdot (2\pi f_{\mathrm{obs}})^2}\,. \tag{13}$$

With the linearization, the capacitances of the resonant circuits can be expressed as

$$C_i(p_i) \approx C_{0,i} + \frac{dC_i}{dp}\Big|_{p_{0,i}} \cdot (p_i - p_{0,i}) \tag{14}$$

and the corresponding pressures as

$$p_i(t) \approx p_{0,i} + \frac{dp}{dt}\Big|_{t_i} \cdot (t - t_i) \tag{15}$$

with

$$p_{0,i} = p|_{C_i = C_{0,i}} \tag{16}$$

and

$$t_i = t|_{p_i = p_{0,i}}\,. \tag{17}$$

Equation (8) can be rewritten by including (14) and (15) and taking (11) and (13) into account:

$$\begin{aligned}
&\Delta f_{res}(t)\\
&\approx \frac{1}{2\pi}\left\{L_2\left[C_{0,2} + \frac{dC_2}{dp}\Big|_{p_{0,2}} \cdot (p_2(t) - p_{0,2})\right]\right\}^{-\frac{1}{2}}\\
&\quad - \frac{1}{2\pi}\left\{L_1\left[C_{0,1} + \frac{dC_1}{dp}\Big|_{p_{0,1}} \cdot (p_1(t) - p_{0,1})\right]\right\}^{-\frac{1}{2}}\\
&\approx \frac{1}{2\pi}\left\{L_2\left[C_{0,2} + \frac{dC_2}{dp}\Big|_{p_{0,2}} \frac{dp_2}{dt}\Big|_{t_2} \cdot (t - t_2)\right]\right\}^{-\frac{1}{2}}\\
&\quad - \frac{1}{2\pi}\left\{L_1\left[C_{0,1} + \frac{dC_1}{dp}\Big|_{p_{0,1}} \frac{dp_1}{dt}\Big|_{t_1} \cdot (t - t_1)\right]\right\}^{-\frac{1}{2}}\\
&= f_{\mathrm{obs}} \cdot \left[1 + \frac{1}{C_{0,2}} \frac{dC_2}{dp}\Big|_{p_{0,2}} \frac{dp_2}{dt}\Big|_{t_2} \cdot (t - t_2)\right]^{-\frac{1}{2}}\\
&\quad - f_{\mathrm{obs}} \cdot \left[1 + \frac{1}{C_{0,1}} \frac{dC_1}{dp}\Big|_{p_{0,1}} \frac{dp_1}{dt}\Big|_{t_1} \cdot (t - t_1)\right]^{-\frac{1}{2}}\,.
\end{aligned} \tag{18}$$

It is preferable that both transponders are identical for the triggering condition to be reached at the same pressure and thus obtain a correct value of the pulse transit time. Thus, for the following investigation of the design, it is assumed that $L_1 = L_2 = L$, $p_{0,1} = p_{0,2} = p_0$, $C_1(p) = C_2(p) = C(p)$ and $C_{0,1} = C_{0,2} = C_0$. Equation (18) is then simplified to

$$\begin{aligned}
\Delta f_{\mathrm{res}} \approx\ & f_{\mathrm{obs}} \cdot \left[1 + \frac{1}{C_0} \frac{dC}{dp}\Big|_{p_0} \frac{dp_2}{dt}\Big|_{t_2} \cdot (t - t_2)\right]^{-\frac{1}{2}}\\
& - f_{\mathrm{obs}} \cdot \left[1 + \frac{1}{C_0} \frac{dC}{dp}\Big|_{p_0} \frac{dp_1}{dt}\Big|_{t_1} \cdot (t - t_1)\right]^{-\frac{1}{2}}\,.
\end{aligned} \tag{19}$$

Additionally, it is assumed that the pulse pressure curve does not change when travelling through the stent, which induces that the pressures at both sensors are the same but time shifted by Δt:

$$p_2(t) = p_1(t - \Delta t) = p(t - \Delta t)\,. \tag{20}$$

This assumption implies that any wave reflections are neglected, which is a realistic assumption, as the shortest wave length of the spectrum of the pulse wave is usually much longer than the stent. In this case the pulse pressure curves have the same slope at the triggering points:

$$\frac{dp_1}{dt}\Big|_{t_1} = \frac{dp_2}{dt}\Big|_{t_2} = \frac{dp}{dt}\Big|_{t_1}\,. \tag{21}$$

With (21) and

$$t_2 = t_1 + \Delta t \tag{22}$$

(19) can be transformed further:

$$\begin{aligned}
\Delta f_{\mathrm{res}}(t) \approx f_{\mathrm{obs}} \cdot \Bigg\{ & \left[1 + \frac{1}{C_0} \frac{dC}{dp}\Big|_{p_0} \frac{dp}{dt}\Big|_{t_1} \cdot (t - t_1 - \Delta t)\right]^{-\frac{1}{2}}\\
& - \left[1 + \frac{1}{C_0} \frac{dC}{dp}\Big|_{p_0} \frac{dp}{dt}\Big|_{t_1} \cdot (t - t_1)\right]^{-\frac{1}{2}}\Bigg\}\,.
\end{aligned} \tag{23}$$

From the derivative of (23) with respect to t it can be shown that $\Delta f_{\mathrm{res}}(t)$ is monotonically decreasing over t in the interval T_{M}, given that ${}^{dC}/_{dp}$ is positive. Thus, $\Delta f_{\mathrm{res,min}}$ is reached at the right border of the interval T_{M}, when $t = t_2 = t_1 + \Delta t$. From this follows

$$\begin{aligned}
\Delta f_{\mathrm{res,min}} &= \Delta f_{\mathrm{res}}\,(t_1 + \Delta t)\\
&= f_{\mathrm{obs}} \cdot \left\{1 - \left[1 + \frac{1}{C_0} \frac{dC}{dp}\Big|_{p_0} \frac{dp}{dt}\Big|_{t_1} \cdot \Delta t\right]^{-\frac{1}{2}}\right\}\,.
\end{aligned} \tag{24}$$

As the transponders were assumed to be identical $B_1 = B_2 = B$ applies and the requirement (9) becomes

$$B \le \Delta f_{\mathrm{res,min}}\,. \tag{25}$$

The $3\,\mathrm{dB}$ bandwidth is related to the quality factor Q and the resonance frequency f_{res} as described by the formula

$$Q = \frac{f_{\mathrm{res}}}{B}\,. \tag{26}$$

Solving (24) for Δt leads to a simple expression for the minimal time difference that can be resolved:

$$\Delta t \ge \frac{C_0}{\frac{dC}{dp}\Big|_{p_0} \frac{dp}{dt}\Big|_{t_1}} \cdot \left[\left(\frac{Q}{Q-1}\right)^2 - 1\right] =: \Delta t_{\mathrm{min}}\,. \tag{27}$$

V. Evaluation

A. Set-up description

An experimental set-up has been realized to validate the presented model and to show that (27) describes the minimum resolvable time difference for the case of identical transponders as claimed. It has been realized in a way that it represents a realistic scenario but does not require any complex or expensive manufacturing technology. In this set-up, the pressure sensors of the transponders that are to be implanted inside a blood vessel are emulated by varactor diodes. Fig. 5 shows the circuit schematics used for each transponder. L_S represents the transponder coil coupled to the transceiver coil. It is implemented as a flat coil with the geometry shown in Fig. 6 and a copper thickness of $35\,\mu\mathrm{m}$ integrated into a circuit board. The dimensions have been chosen for a stent

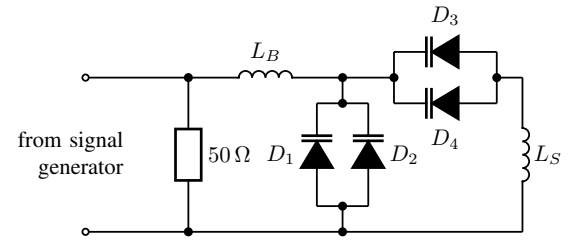

Fig. 5. Transponder circuit

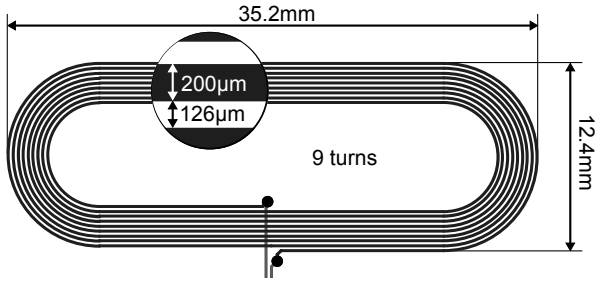

Fig. 6. Transponder coil dimensions

that has a diameter of $6\,\mathrm{mm}$ and a length of $80\,\mathrm{mm}$. These are typical dimensions for peripheral stents [24]. If the coil were manufactured on a flexible substrate and bent around its longitudinal axis to the specified diameter, it would form a saddle coil with its conductors being located on opposite sides of the stent, thus having a large cross section to interact with the transceiver coil field. The four varactor diodes D_1 to D_4 emulate the capacitive pressure sensors. A back-to-back configuration has been chosen in order to reduce distortion due to the non-linearity of the voltage / capacitance characteristics. To compensate for the accompanied reduction of capacitance, two diodes have been connected in parallel in each branch. Their capacitance is controlled by a signal generator. The RF signal coupled in from the transceiver coil is blocked from this signal generator by the inductor L_B.

The chosen set-up that represents the readout unit is shown schematically in Fig. 7. A digital lock-in amplifier (Zurich Instruments HF2LI) is used as an RF-signal generator and measures phase and magnitude of the measurement signal in reference to the applied signal. The transceiver coil has been realized as a wire loop with a diameter of $10\,\mathrm{cm}$. A directional coupler (Mini-Circuits ZFDC-10-1B-S+) is inserted between the transceiver coil and the signal output of the lock-in amplifier. It directs the signal reflected at the coil to its couple port, which serves as the measurement signal transferred to the lock-in amplifier's input.

B. Set-up characterization

The developed transponders have the measured voltage / resonance frequency characteristics shown in Fig. 8. To model the pressure sensors the characteristic curve shown in Fig. 9 is used. It has been derived from the basic model for a MEMS capacitive pressure sensor in [25, p. 299 *et seq.*] with realistically chosen values given in the Appendix. The inductance L of a bare transponder coil has been measured

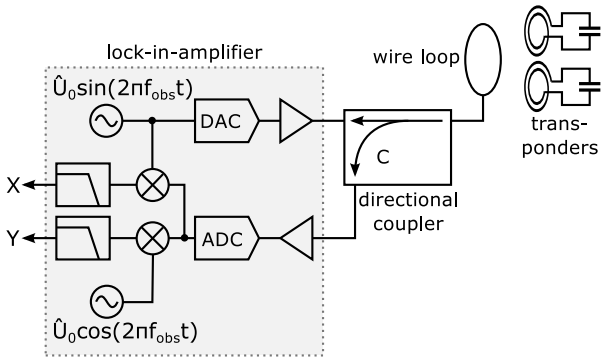

Fig. 7. Measurement setup schematics

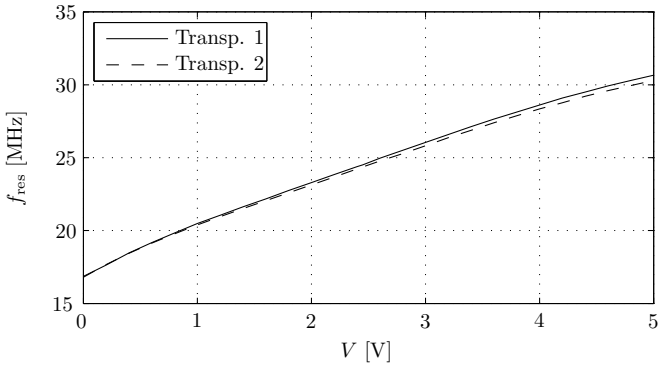

Fig. 8. Voltage / resonance frequency characteristics of the transponders circuits

by means of an impedance analyzer connected directly to its terminals. Both transponders are intended to trigger at the pressure of $p_0 = 100\,\mathrm{mmHg}$. This pressure corresponds to a capacitance of $C_0 = 10.5\,\mathrm{pF}$ and a resonance frequency of $f_\mathrm{obs} = 25.37\,\mathrm{MHz}$. The time t_1 at which p_0 occurs at sensor 1 at the rising edge of the pulse curve could be obtained from Fig. 2. The quality factor of the transponder coils has been obtained by combining a coil with a fixed capacitor to form a series resonant circuit and measuring its impedance. A model has been fit to the data to estimate the quality factor at resonance, which has been transferred to the measurement frequency f_obs. It is assumed that the coil dominates the losses, thus losses in capacitor or varactor diodes can be neglected. Table I summarizes the obtained coil parameters used for evaluation.

By combining the pulse wave signal from Fig. 2, the pressure sensor characteristics from Fig. 9 and the coil parameters

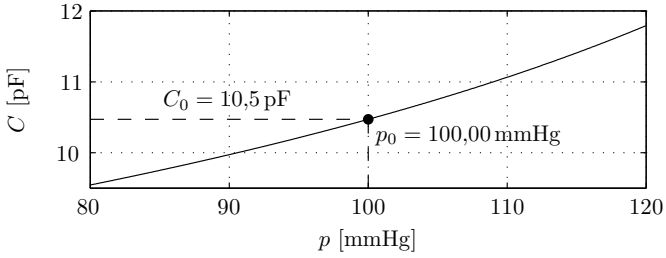

Fig. 9. Pressure sensor characteristics

TABLE I
TRANSPONDER COIL PROPERTIES

Symbol	Value	Comment
L	3.76 µH	At 27 MHz
Q	79.6	At f_{obs} (see text)

from Table I, the voltage signal that has to be applied to the transponder circuits to emulate the pressure signal is obtained.

To validate the criterion (27), the formula is applied to the experimental set-up. Therefore, the slopes of the pulse wave signal and the sensitivity of the pressure sensor at the trigger pressure have been obtained from the characteristics. Table II summarizes all values used for the calculation of the theoretical minimal transit time. The result is:

$$\Delta t_{\min} = 8.56\,\mathrm{ms}\,. \tag{28}$$

TABLE II
PARAMETERS USED FOR ESTIMATION OF MINIMUM TRANSIT TIME

Symbol	Value	Comment
p_0	100 mmHg	
C_0	10.5 pF	Taken from pressure sensor characteristics depicted in Fig. 9
t_1	49.5 ms	Taken from pressure curve depicted in Fig. 2 and 3
$dC/dp\big\|_{p_0}$	54 fF · mmHg^{-1}	Obtained from pressure sensor characteristics depicted in Fig. 9
$dp/dt\big\|_{t_1}$	580 mmHg · s^{-1}	Obtained from pressure curve depicted in Fig. 2

C. Execution

Fig. 11 shows the actual arrangement of transceiver coil and transponders for the measurement. The transponder coils have been aligned symmetrically with respect to the transceiver coil axis as can be seen in Fig. 11b and the coil planes are parallel. The distance between transceiver coil and transponder coils is approximately 47 mm. The transponder coils have a center distance of 36.8 mm and a minimal distance of only 1.6 mm, which results in strong coupling. Although this effect could be integrated into the model, it has been decided to reduce it to minimize the number of parameters. One option to achieve this would be to separate the transponders. Here instead, it has been decided to add a grounded shield between the coils. It consists of two sheets of copper foil, one on each side of the PCB, which are attached perpendicularly to the PCB and electrically connected with a solder point at the PCB edge (see Fig. 10b). The shield is further soldered to the ground rail of each transponder (lower line in Fig. 6) with two pieces of magnet wire (see Fig. 10a). The ground rails are connected to the ground of the signal generator.

The varactors of the transponder circuits are supplied with the voltage signal obtained as described in section V-B. Therefore, the waveform has been generated by a Matlab script and loaded into a 2-channel arbitrary signal generator. The synchronization output of the signal generator has been used as a trigger input during data acquisition. The signal sent to transponder 2 is delayed by the assumed pulse transit time Δt.

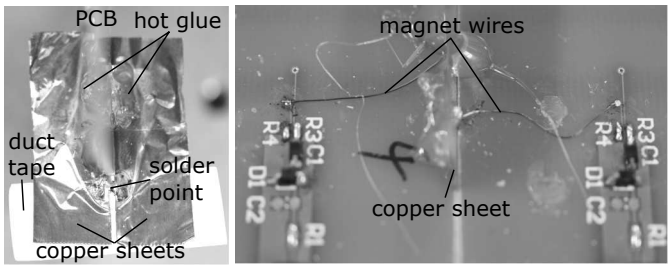

(a) Side view (b) Front view

Fig. 10. Shielding method

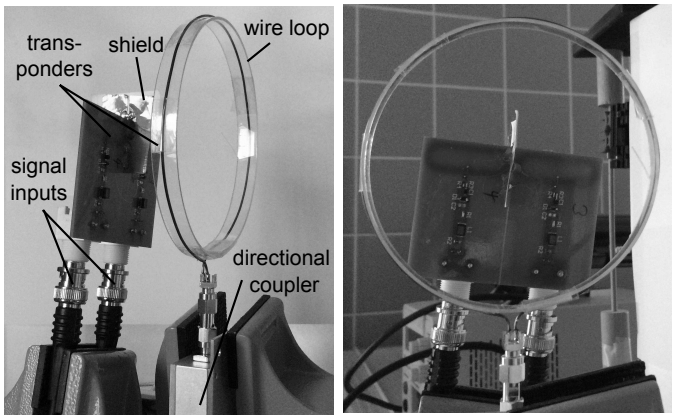

(a) Side view (b) Front view

Fig. 11. Measurement set-up

The experiment has been executed with the parameters shown in Table III. Three different values for the transit time

TABLE III
PARAMETERS USED FOR MEASUREMENT

Symbol	Value	Comment
f_{obs}	25.37 MHz	Calculated from C_0 and L using (4)
$\hat{U}_0$	1 V	
n_{LI}	8	Lock-in amplifier low pass filter order
$f_{\mathrm{c,LI}}$	9.6 kHz	Lock-in amplifier low pass filter −3 dB corner frequency

have been examined, which are spread closely around the calculated limit $\Delta t_{\min}$:

- $\Delta t = 7\,\mathrm{ms}$ (dashed line in the upcoming figures),
- $\Delta t = 8\,\mathrm{ms}$ (solid line in the upcoming figures), and
- $\Delta t = 9\,\mathrm{ms}$ (dash-dotted line in the upcoming figures).

Fig. 12a shows the virtual pressures applied to the two transponders for the different values.

D. Results

Fig. 12b shows the measured output signal of the lock-in amplifier, which corresponds with the signals X and Y in Fig. 7 as follows:

$$\begin{aligned} |\underline{V}_{\mathrm{LI}}| &= \sqrt{(X^2+Y^2)/2} \\ \angle\{\underline{V}_{\mathrm{LI}}\} &= \tan^{-1}(Y/X)\,. \end{aligned} \tag{29}$$

The triggering conditions when the pressures cross $p_0 = 100\,\mathrm{mmHg}$ around $50\,\mathrm{ms}$ and $325\,\mathrm{ms}$ are clearly visible. However, the individual instants when sensor one and sensor 2 trigger can hardly be distinguished at that scale, so Fig. 13a shows the area near the rising edge of the pressure signal in greater detail. In this figure, the resonances of both transponders are visible both in magnitude and in phase of $\underline{V}_{\mathrm{LI}}$ as dips in the signal. We would expect that for values of Δt below $\Delta t_{\min}$ the two dips of the resonances cannot be distinguished. The following was found: For $\Delta t = 9\,\mathrm{ms}$ two dips are observed, while for $\Delta t = 7\,\mathrm{ms}$ magnitude and phase are monotonically decreasing or increasing in the complete measurement interval. For $\Delta t = 8\,\mathrm{ms}$ they almost show a saddle point in between. However, the dips do not occur exactly at the theoretical position of t_1 and t_2. This is supposed to be due to some delay in the trigger circuit or offset in the varactor modulation voltages.

For evaluation, the expected output signals have also been calculated from the model. To do this, more parameters had to be determined: inductance and series resistance of the transceiver coil (L_{P}, R_{P}) and the mutual inductances (or coupling factors respectively) between the coils (M_1, M_2, M_3). The former values could be measured with an impedance analyzer. The mutual inductances have been iteratively adjusted such that the simulation outcome resembled the measured results as closely as possible, while assuming that the coupling between the transponder coils and the transceiver coil (M_1 and M_2) are the same due to their symmetric geometrical position related to the transceiver coil axis. Despite shielding, k_3 can not be assumed to be 0 for a suitable fit. It has been observed that M_1 and M_2 affect the depth of both dips, while M_3 mainly affects the difference of depth between the two dips, which helped in making the adjustment. Therefore, the coupling between transceiver coil and transponder coils does not affect the relative depth of the dips. Table IV shows the final values for the additional parameters needed for simulation. The results for the expected lock-in amplifier output signal have been plotted besides the measured signals in Fig. 13b.

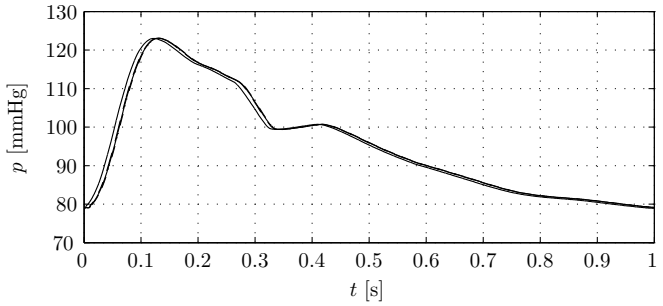

(a) Pressure at transponder 1 (very left line) and transponder 2 for different values of Δt (very close lines at the right)

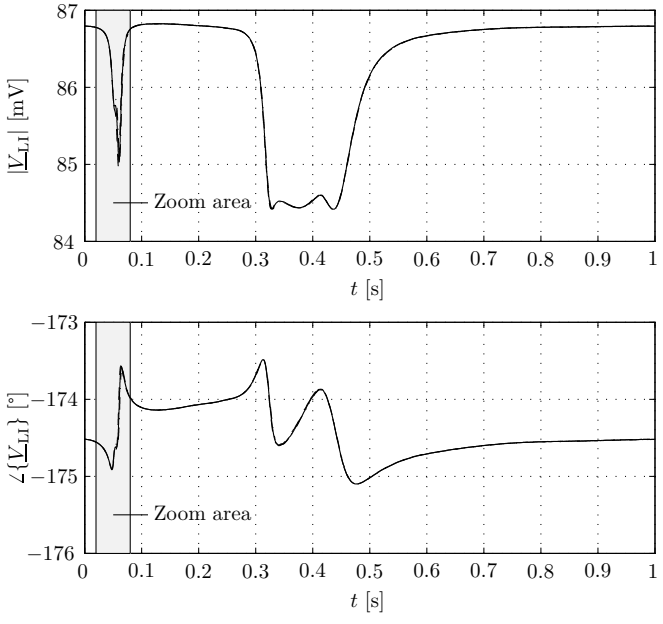

(b) Measured output signal of lock-in amplifier for different values of Δt

Fig. 12. Simulated pressure signals and output signal of lock-in amplifier for different values of Δt over full pulse period

TABLE IV
FURTHER PARAMETERS USED FOR SIMULATION

Symbol	Value	Comment
L_{P}	0.32 µH	Measured at f_{obs}
R_{P}	0.15 Ω	Measured at f_{obs}
C	−10.5 dB	Nominal value from data-sheet
M_1	13.2 nH	Coupling factor $k_1 = 0.012$ (see text)
M_2	13.2 nH	Coupling factor $k_2 = 0.012$ (see text)
M_3	−18 nH	Coupling factor $k_3 = -0.0048$ (see text)

The conditions used for simulation match exactly the conditions applied when calculating the minimum transit time. It can be seen that with the adoption of the coupling parameters the qualitative course of the simulated signals resemble the measured signals very well, suggesting that the model structure is suitable. Now the dips of the magnitude also correspond to the theoretical values of t_1 and t_2. That there is a large offset in phase between measured and simulated signal is to be expected due to transit delay through the cabling and the phase shift imposed by the coupler: The coupler introduces a phase shift of 180° between its in- and couple-port, while between in- and out-port the phase shift is almost 0°. The cabling between signal output and input of the lock-in amplifier has a total length of $2\,\mathrm{m}$, which adds 91° for the given measurement frequency and a velocity factor of 0.67. The total expected phase shift adds up to 271°, which is close to the observed phase shift between calculated and measured signal in Fig. 13 of about 263°.

The behavior of the system also becomes clear when examining the phenomenon in the frequency domain: Figs. 14a and 14b show the measured and simulated impedance at the transceiver coil obtained under static conditions corresponding to the time when the first sensor is at trigger pressure ($t = t_1$; $p_1 = p_0$). The second sensor is at the pressure value that corresponds to the time $t_1 + \Delta t$ for the investigated values of Δt. The measured plots have been obtained with an impedance analyzer. Again the phase shows the distinct dips that correspond to the two transponders' resonance frequencies.

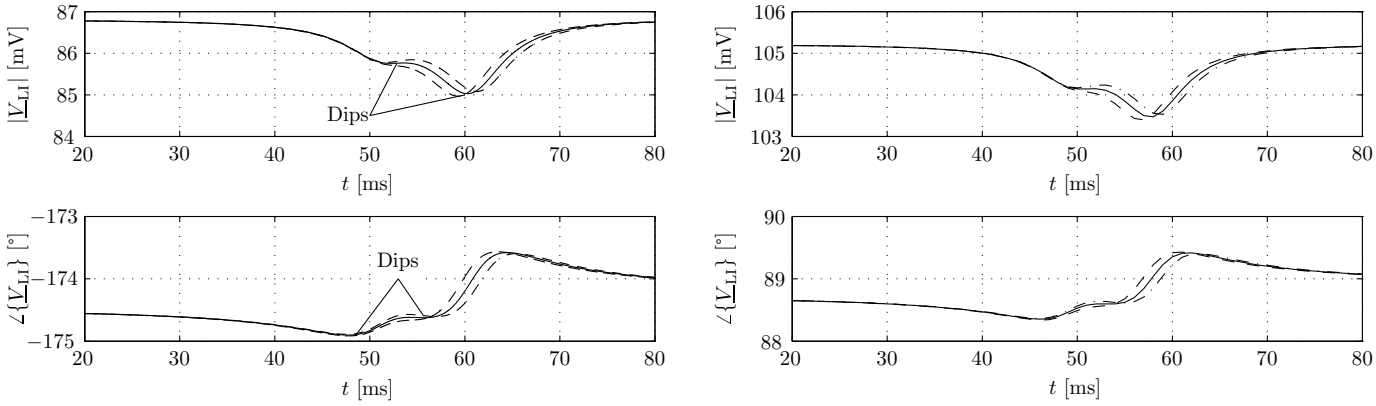

(a) Measured (b) Simulated

Fig. 13. Zoomed view of output signal of lock-in amplifier for different values of Δt

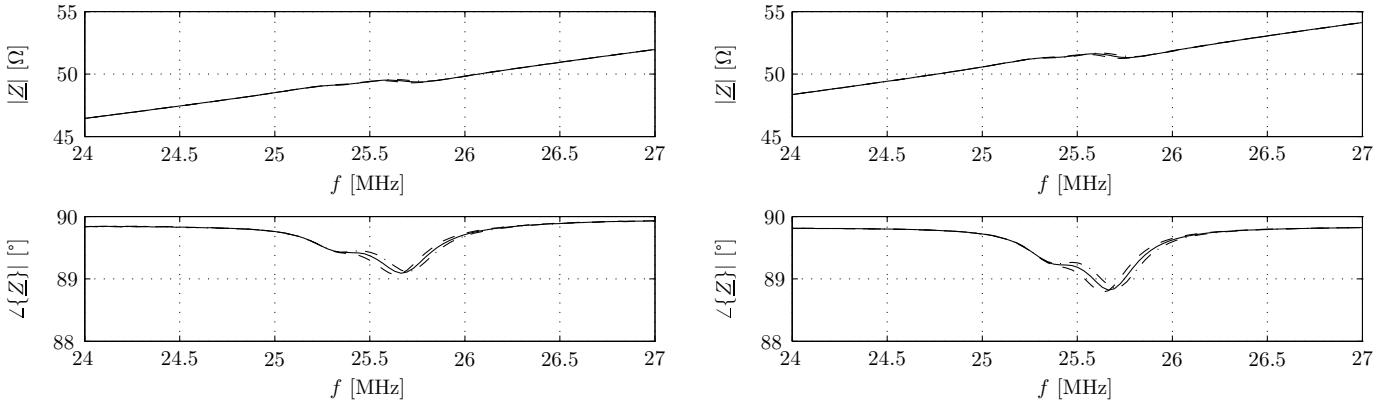

(a) Measured (b) Simulated

Fig. 14. Impedance at transceiver coil for $t = t_1$ and different values of Δt

VI. Resulting implications on the transponder design

The major challenge for the electrical design is to separate the resonances of the transponders such that an appropriate time distance can be resolved. Equation (27) contains information on the design parameters of the transponders that influence this value. They have limits: The transponder quality factor Q can not be arbitrarily high. It is limited by different kinds of power losses, e.g. due to eddy currents and direct conductor losses. Yet the requirement on Δt (27) reveals other parameters that can be adjusted in order to achieve the design goal. Table V summarizes these and contains the direction in which the parameters relate to the separation of the resonances. The other design parameters are also limited. The PWV cannot be influenced, neither can the derivative of the pulse pressure curve ${}^{dp}/_{dt}|_{t_1}$. The distance of the sensors d is limited by the length of the stent, which it cannot exceed. The sensitivity of the pressure sensors ${}^{dC}/_{dp}|_{p_0}$ can be increased by enlarging the membrane (or use several membranes in parallel), which increases the physical size, or by decreasing the membrane thickness, reducing its stability. There is also the option of using a less stiff material. The sensor capacitance at resonance C_0 can most easily be reduced by increasing the separation of the membrane electrodes. This will, at the same time, reduce the sensitivity, so a compromise has to be found. The observation frequency is limited by regulatory requirements, interference with other devices and interaction with body tissue. At high frequencies, the penetration depth of the magnetic field into the body decreases due to the skin effect. On the other hand, with increasing frequency L and C decrease, which allows for smaller dimensions of the transponder. As physical dimensions will be critical for the application, the frequency should be chosen as high as possible within suitable penetration depth. From other investigations it can be concluded that 10 MHz to 30 MHz is a suitable range [26], [27]. It is further proposed to maximize the inductance L of the transponder coils to the geometrical limits. The pressure sensors have to be designed to an appropriate value of S_{C} given by (27) and the desired value of C_0 given by (12).

VII. Discussion

The measured signals on the experimental set-up are in good agreement with the simulation. The electrical model of the inductive transmission therefore is considered to be valid. Moreover, the signals showed that the characteristic features

TABLE V
PARAMETERS THAT INFLUENCE THE SEPARATION OF THE RESONANCES

Quantity	Symbol	Sense*	Limits
Pulse wave velocity	PWV	-	None
Distance of the sensors	d	+	Limited by stent length
Derivative of the pulse wave curve at triggering point	$dp/dt\big\|_{t_1}$	+	None
Sensitivity of the pressure sensors at triggering point	$dC/dp\big\|_{p_0}$	+	Limited by membrane size and stability
Capacitance of the pressure sensors at triggering point	C_0	-	Trade-of with sensitivity has to be found†
Transponder inductance	L	+	Limited by geometrical boundaries†
Observation frequency	f_{obs}	+	Limited by requirements to temporal resolution, regulatory requirements and interaction with body tissue†
Transponder quality factor	Q	-	Limited by losses

* "+": the higher the value, the better the separation; "-": the lower the value, the better the separation.
† f_{obs}, C_0 and L cannot be chosen independently. They are dependent as described by (12).

of the measured signal (e.g. local minima in the phase of the reflected signal) disappear, when the transit time falls below the value predicted by the requirement (27).

The experimental set-up has not been optimized for a low resolvable transit time, so the $\Delta t_{\min}$ reached in the experiment is low for a practical application. Assuming that the maximum PWV we want to measure is $10\,\mathrm{m}\cdot\mathrm{s}^{-1}$, which is an optimistic yet realistic value, then the distance between the sensors d must not be lower than $86\,\mathrm{mm}$. For a peripheral stent that is still a reasonable length (see [24]). Nevertheless, the set-up is based on an ideal case: the transmission took place in air, the alignment was symmetric and coupling between the transponders has been reduced by shielding. The surrounding tissue and stent material would affect $\Delta t_{\min}$ adversely: they cause loss and therefore decrease the quality and the coupling factors. This leads to wider and less expressed ripples and dips in magnitude and phase of the measured signal, both in the frequency and in the time domain. The tissue effect is to a great extent caused by eddy losses in the surrounding tissue, which is conductive. It is dependent on the position of the stent within the body and is patient specific. The conductivity is also a function of time. In order to study the effect of tissue on coupling and quality factors, FEA calculations or experiments with animal tissue are suggested. Once real values for quality and coupling factors are known, the influence can be considered in a practical design. An asymmetry of the alignment would lead to different dip depths for both transponders, as does coupling between the transponders. Placing a shield to decouple the transponder coils is most likely not an option in a real stent. The coils have to be separated spatially (losing available space), or the coupling has to be taken into account in the design. It must also be considered that the slope of the pulse pressure curve can be lower in practice, especially in pathological cases. The presented model allows to study the effect of such variations.

To optimize the proposed measurement system further, micro manufacturing methods should be taken into consideration. They are necessary to realize a coil that fits into a coronary stent while achieving sufficient inductance. Pressure sensors with very high sensitivity, e.g. with polymer based diaphragms, could be necessary.

Apart from optimization, future work comprises the definition of a strategy to obtain the trigger instances from the measurement signal. One suggested approach is to search for minima of the phase of the lock-in amplifier signal, e.g. by searching for zeros in its derivative.

The influence of signal noise is also an important subject for further investigations. Noise determines the lower limit of the coupling factor up to which the resonances can be detected before they vanish in the noise floor. Furthermore, it introduces a statistical error on the measured transit time and therefore influences the precision of the measurement. An approach to take this into account is to model the noise as Gaussian distributed and band limited to the lock-in amplifier's filter bandwidth. Once the approach for resonance detection is defined, the influence of such noise on the determined pulse transit time can be studied mathematically.

The integration of the transponders into the stent is another research subject. The approach published by Takahata *et al.*, which also makes use of the stent structure as an antenna, is appealing [9]. An alternative is to integrate coil and sensor on a flexible polyimide substrate which is wrapped around the stent [28]. With this approach it has to be considered that the bending curvature of the coil will change its characteristics. The effective cross-section is reduced, which reduces coupling and inductance. The equivalent series resistance is also expected to change slightly due to proximity effect. Further challenges are that the transponders may not disturb blood flow and they must both survive and not obstruct the implantation process, during which the stent is compressed to a diameter much less than in its expanded state.

Medical questions are other subjects to further investigations. They include how fast the pulse wave will actually be in a blood vessel stiffened by a stent and how the sensors will be covered with biological material. If both sensors are asymmetrically covered with cells, their sensitivity differs, which leads to a change in the apparent transit time. The proposed sensor system provides a value for the mean PWV inside the stent. It is not designed to differentiate between different shapes of restenosis[6].

The advantage of the proposed PWV-based method compared to pressure-based methods is revealed when considering a decrease in pressure sensor sensitivity due to coverage of the sensors. It has two effects: An increase in triggering pressure and a change in slope at the triggering condition. As long as the sensors are affected identically and the pulse

[6]E.g. focal, diffuse, proliferative as defined in [29]

wave does not change its form between the sensors, a slight change in trigger frequency is compensated as the triggering times are subtracted. For a substantial change in sensitivity the observation frequency can be adapted, so that it is still crossed by the resonance frequencies. Therefore, the PWV-based concept is robust to sensitivity changes as long they affect both sensors identically. However, the decrease in slope increases the minimum resolvable transit time. If a range for the slope change can be quantified, it may be considered in the design.

VIII. Conclusion

This investigation aimed to determine the electronic design criteria for an implantable PWV measurement system based on resonance detection on LC-transponders. The model and the requirements obtained in this article deliver a starting point for the design of such an implantable PWV measurement system. Given that the bandwidths of the transponders' resonance peaks may not overlap (9), a design criterion on the minimal transit time (27) has been derived for the preferable case that both transponders are equal. The qualitative and quantitative similarity between measured and simulated results and the fact that in simulation the signals show the expected behavior suggest that the requirement on the transit time (27) yields suitable results for this measurement task. If it is fulfilled, the signal measured by the lock-in amplifier would, with some signal processing (e.g. calculation of its derivative), yield a proper triggering signal to measure the pulse transit time and, with known distance of the sensors, PWV.

Appendix
Capacitive pressure sensor model

The model for the capacitive pressure sensors used in the evaluation has been found in [25, p. 299 *et seq.*]. In addition, to increase sensitivity, N sensor structures have been virtually connected in parallel. The parameters in Table VI have been used.

TABLE VI
Parameters used for the capacitive pressure sensor model

Quantity	Symbol	Value
Membrane radius	r_a	120 µm
Membrane thickness	h	2 µm
Young's modulus of membrane	Y	150 GPa
Poisson ratio of membrane	ν	0.15
Distance of the electrodes (without deformation)	d	0.7 µm
Counter electrode diameter	αr_a	108 µm
Reference pressure	p_0	1013.25 hPa
Number of sensors in parallel	N	16

The capacitance is obtained from

$$C(u_0) = N \int_0^{\alpha r_\mathrm{a}} \epsilon_0 \frac{2\pi r}{d - u_0 \left(1 - \left(r \,/\, r_\mathrm{a}\right)^2\right)^2} \, dr \tag{30}$$

with

$$u_0 = \frac{r_\mathrm{a}^4}{64D} \left(p - p_0\right) \tag{31}$$

and

$$D = \frac{Y h^3}{12\left(1 - \nu^2\right)} . \tag{32}$$

Acknowledgement

The author would like to thank A. Domnich, V. Schrader, A. van Poelgeest and J. Stallkamp for their support.

References

[1] G. A. Fishbein and M. C. Fishbein, "Arteriosclerosis: rethinking the current classification." *Archives of pathology & laboratory medicine*, vol. 133, no. 8, pp. 1309–16, Aug. 2009.

[2] J. W. Jukema, J. J. W. Verschuren, T. A. N. Ahmed, and P. H. A. Quax, "Restenosis after PCI. Part 1: pathophysiology and risk factors." *Nature reviews. Cardiology*, vol. 9, no. 1, pp. 53–62, Jan. 2012.

[3] T. Inoue, K. Croce, T. Morooka, M. Sakuma, K. Node, and D. I. Simon, "Vascular inflammation and repair: implications for re-endothelialization, restenosis, and stent thrombosis." *JACC. Cardiovascular interventions*, vol. 4, no. 10, pp. 1057–66, Oct. 2011.

[4] J. W. Jukema, T. A. N. Ahmed, J. J. W. Verschuren, and P. H. A. Quax, "Restenosis after PCI. Part 2: prevention and therapy." *Nature reviews. Cardiology*, vol. 9, no. 2, pp. 79–90, Feb. 2012.

[5] T. Rassaf, S. Steiner, and M. Kelm, "Postoperative care and follow-up after coronary stenting." *Deutsches Ärzteblatt international*, vol. 110, no. 5, pp. 72–81, Feb. 2013.

[6] N. Xu, J. Zhang, M. Li, J. Pan, and Z. Lu, "Incidence and classification of neointimal proliferation and in-stent restenosis in post-stenting patients at 1-year interval: findings from non-invasive coronary computed tomography angiography." *European journal of radiology*, vol. 83, no. 10, pp. 1816–21, Oct. 2014.

[7] E. Y. Chow, A. L. Chlebowski, S. Chakraborty, W. J. Chappell, and P. P. Irazoqui, "Fully Wireless Implantable Cardiovascular Pressure Monitor Integrated with a Medical Stent," *IEEE Transactions on Biomedical Engineering*, vol. 57, no. 6, pp. 1487–1496, Jun. 2010.

[8] K. Takahata, A. DeHennis, K. D. Wise, and Y. B. Gianchandani, "A wireless microsensor for monitoring flow and pressure in a blood vessel utilizing a dual-inductor antenna stent and two pressure sensors," in *17th IEEE International Conference on Micro Electro Mechanical Systems. Maastricht MEMS 2004 Technical Digest*, 2004, pp. 216–219.

[9] K. Takahata, Y. B. Gianchandani, and K. D. Wise, "Micromachined Antenna Stents and Cuffs for Monitoring Intraluminal Pressure and Flow," *Journal of Microelectromechanical Systems*, vol. 15, no. 5, pp. 1289–1298, Oct. 2006.

[10] S. R. Green and Y. B. Gianchandani, "Wireless magnetoelastic monitoring of biliary stents," *Journal of Microelectromechanical Systems*, vol. 18, no. 1, pp. 64–78, 2009.

[11] S. R. Green, R. S. Kwon, G. H. Elta, and Y. B. Gianchandani, "In situ and ex vivo evaluation of a wireless magnetoelastic biliary stent monitoring system." *Biomedical microdevices*, vol. 12, no. 3, pp. 477–84, Jun. 2010.

[12] S. R. Green and Y. B. Gianchandani, "Tailored magnetoelastic sensor geometry for advanced functionality in wireless biliary stent monitoring systems," *Journal of Micromechanics and Microengineering*, vol. 20, no. 7, p. 075040, Jul. 2010.

[13] S. R. Green, R. S. Kwon, G. H. Elta, and Y. B. Gianchandani, "In vivo and in situ evaluation of a wireless magnetoelastic sensor array for plastic biliary stent monitoring." *Biomedical microdevices*, vol. 15, no. 3, pp. 509–17, Jun. 2013.

[14] A. Viswanath, S. R. Green, J. Kosel, and Y. B. Gianchandani, "Metglas-Elgiloy bi-layer, stent cell resonators for wireless monitoring of viscosity and mass loading," *Journal of Micromechanics and Microengineering*, vol. 23, no. 2, p. 025010, Feb. 2013.

[15] J. Schächtele and A. Domnich, "Drahtloses Restenose-Früherkennungssystem mit passiver Sensorik zur Integration in einen Stent," in *4. Dresdner Medizintechnik-Symposium*. Dresden: TUDpress, 2012, pp. 229–232.

[16] A. Domnich and J. Schächtele, "Cylindrical device, pulse wave measurement system and method for measuring a pulse wave speed," 2012.

[17] S. Laurent, J. Cockcroft, L. Van Bortel, P. Boutouyrie, C. Giannattasio, D. Hayoz, B. Pannier, C. Vlachopoulos, I. Wilkinson, and H. Struijker-Boudier, "Expert consensus document on arterial stiffness: methodological issues and clinical applications." *European heart journal*, vol. 27, no. 21, pp. 2588–605, Nov. 2006.

[18] W. W. Nichols, M. F. O'Rourke, and C. Vlachopoulos, *McDonald's Blood Flow in Arteries: Theoretical, Experimental and Clinical Principles*, 6th ed. Boca Raton: Taylor & Francis Group, 2011.
[19] J. C. Bramwell and A. V. Hill, "The Velocity of the Pulse Wave in Man," *Proceedings of the Royal Society B: Biological Sciences*, vol. 93, no. 652, pp. 298–306, Apr. 1922.
[20] K. S. Heffernan, W. K. Lefferts, and J. A. Augustine, "Hemodynamic correlates of late systolic flow velocity augmentation in the carotid artery." *International journal of hypertension*, vol. 2013, Jan. 2013.
[21] R. Nopper, R. Niekrawietz, and L. Reindl, "Wireless Readout of Passive Sensors," *IEEE Transactions on Instrumentation and Measurement*, vol. 59, no. 9, pp. 2450–2457, Sep. 2010.
[22] O. Akar, T. Akin, and K. Najafi, "A wireless batch sealed absolute capacitive pressure sensor," *Sensors and Actuators A: Physical*, vol. 95, no. 1, pp. 29–38, Dec. 2001.
[23] C. Bowick, *RF circuit design*, 2nd ed. Newnes, 2007.
[24] M. Singh, B. J. Gersh, R. L. McClelland, K. K. L. Ho, J. T. Willerson, W. F. Penny, and D. R. Holmes, "Clinical and angiographic predictors of restenosis after percutaneous coronary intervention: insights from the Prevention of Restenosis With Tranilast and Its Outcomes (PRESTO) trial." *Circulation*, vol. 109, no. 22, pp. 2727–31, Jun. 2004.
[25] T. B. Jones and N. G. Nenadic, *Electromechanics and MEMS*. Cambridge: Cambridge University Press, 2013.
[26] E. S. Hochmair, "System optimization for improved accuracy in transcutaneous signal and power transmission." *IEEE transactions on biomedical engineering*, vol. 31, no. 2, pp. 177–86, Feb. 1984.
[27] P. Vaillancourt, A. Djemouai, J. F. Harvey, and M. Sawan, "EM radiation behavior upon biological tissues in a radio-frequency power transfer link for a cortical visual implant," in *Proceedings of the 19th Annual International Conference of the IEEE Engineering in Medicine and Biology Society. 'Magnificent Milestones and Emerging Opportunities in Medical Engineering' (Cat. No.97CH36136)*, vol. 6, no. C. IEEE, 1997, pp. 2499–2502.
[28] C. C. Oliveira, A. T. Sepulveda, N. Almeida, B. L. Wardle, J. M. da Silva, and L. A. Rocha, "Implantable Flexible Pressure Measurement System Based on Inductive Coupling." *IEEE transactions on biomedical engineering*, vol. 62, no. 2, pp. 680–687, Feb. 2015.
[29] R. Mehran, G. Dangas, A. S. Abizaid, G. S. Mintz, A. J. Lansky, L. F. Satler, A. D. Pichard, K. M. Kent, G. W. Stone, and M. B. Leon, "Angiographic Patterns of In-Stent Restenosis : Classification and Implications for Long-Term Outcome," *Circulation*, vol. 100, no. 18, pp. 1872–1878, Nov. 1999.

Jonathan Schächtele studied mechatronics at the Friedrich-Alexander Universität Erlangen-Nürnberg, Germany, where he received his Dipl.-Ing. degree with distinction in 2009.

Since then, he has been working as a research assistant at the Fraunhofer Institute for Manufacturing Engineering and Automation (IPA). From 2009 to 2012 he was with the department for Production and Process Automation in Stuttgart, Germany. In 2012 he switched to the newly founded Project Group for Automation in Medicine and Biotechnology in Mannheim, Germany, where he is a project manager within the research group Control Systems in Medical Engineering. His focus is on micro sensor and actuator systems for active implantable devices and surgical instruments.